GEOPHYSICAL RESEARCH LETTERS, VOL. 24, NO. 22, PP. 2817–2820, 1997

Global ocean thermohaline conveyor at present and in the late Quaternary

Dan Seidov

Earth System Science Center, Pennsylvania State University, University Park, USA

Bernd J. Haupt

Sonderforschungsbereich 313, Universität Kiel, Kiel, Germany

Abstract. Operation modes of the global ocean thermohaline conveyor at present, at the last glacial maximum, and at a subsequent meltwater event (MWE) are revisited using a combination of a global ocean circulation model and a semi–Lagrangian trajectory tracing model. The trajectory tracing model helps to visualize the true three–dimensional water transport that is not accessible within traditional ocean circulation modeling. Our simulations confirm that the glacial mode of the conveyor was substantially weaker as compared to the present day mode. However, the simulations indicate that major changes of the deep global ocean conveyor occurred only at the MWE. These changes led to reversal of the Indian–Atlantic branch of the deep conveyor due to complete cessation of North Atlantic Deep Water production caused by a very localized meltwater impact.

Introduction

The present–day paradigm of ocean climate dynamics implies [Gordon et al., 1992] that the global ocean thermohaline circulation system, also known as the salinity conveyor belt [Broecker and Denton, 1989; Broecker, 1991], is strongly controlled by the production of North Atlantic Deep Water (NADW). Proxy data analysis indicates that this circulation system has undergone drastic changes [e.g., Broecker and Denton, 1989]. Moreover, various evidence shows that the ocean circulation has varied between two or three main states, or "modes," strongly controlled by a freshwater impact in the high–latitudinal NA (the reference list is limited here; see extended references in [Seidov et al.,1996] and [Seidov and Haupt, 1997]).

We present the numerical simulation of a response that the ocean conveyor might have had to different sea surface conditions, such as those characteristic of the last glacial maximum (LGM) and a subsequent meltwater event. The term meltwater event (MWE) designates a strong freshening of the northern NA (NNA) near 13,5 k B.P. [Sarnthein et al., 1995]. The core of our approach is a combination of the traditional simulations of the global ocean circulation using an Ocean General Circulation Model (OGCM) and a Lagrangian technique of tracing the water volume transport [Seidov and Haupt, 1997]. An analogous approach has been recently advanced by Drijfhout et al. [1996], who traced the present day global conveyor. A novel feature of the present work is a comparative study of three major glacial–to–interglacial modes of the conveyor employing the combined Eulerian–Lagrangian approach.

The Setup of Numerical Experiments

The numerical experiments have been carried out in two steps. First, the OGCM has been run using the appropriate boundary conditions. In this study we use the GFDL ocean general circulation model [Bryan, 1969; Cox, 1984; Pacanowski et al., 1993]. To reach a steady state in modern and LGM runs, we integrated OGCM for 10,000 years of model time. The duration of the meltwater event is thought to be several hundreds to one thousand years [Sarnthein et al., 1995]. Therefore, the MWE velocity field is the result of integration over only 500 years beginning from the LGM steady state and with the LGM sea surface condition replaced by those appropriate for the MWE. This duration is at the edge of the ocean turnover time, and probably the deep ocean was not totally adjusted to the surface meltwater impact. Although it may take hundreds of years to circulate water globally, the change to the NA overturning occurs almost instantly on the geological time scale (within first 10 years) once the NA convection is capped. This MWE signal is that strong it can easily be traced by an OGCM [Seidov et al., 1996].

In order to facilitate multiple long runs, a coarse resolution (6° longitude by 4° latitude) with 12 levels in vertical is used. It has been noticed that the GFDL model is capable of reproducing the rates of deepwater production and thermohaline overturning fairly well using a rather coarse resolution [Toggweiler et al., 1989]. We have found this to be true with the resolution even coarser than in the cited study. Most of major surface currents, though clearly seen on the vector maps, are substantially (sometimes 2–3 times) weaker than the observed ones, except for Antarctic Circumpolar Current (ACC). However, the meridional thermohaline overturning, which largely depends on the deep convection and isopycnal outcrop, is modeled far better than the horizontal flows. Our present–day convection pattern (not shown) agrees well with that of Toggweiler et al. [1989], and looks rather reasonable. Convection is deep enough to set forth the deep NA conveyor of reasonable intensity. The overturning in the NA is 23 Sv (1 Sv=10^6 m^3/s), and the Antarctic Bottom Water (AABW) inflow into the Atlantic Ocean is about 9 Sv.

We restore the upper layer thermohaline fields to the specified sea surface temperature (SST) and sea surface salinity (SSS). Modern annual mean SST and SSS are specified from new ocean climatological data sets [Levitus and Boyer, 1994; Levitus et al., 1994], except for the Norwegian–Greenland Seas (NGS) and for the area south of Greenland where some additional cooling of up to 2°C was needed to obtain present–day annual NADW production. The LGM SST and SSS were specified as follows: (1) everywhere, except for the NA to the north of 10°N, the CLIMAP [1981] SST were used; (2) everywhere, except for the same area in the NA, the

present day SSS was increased by 1 psu to reflect a consequence of a 120 m sea level drop during the LGM [Duplessy et al., 1991]; (3) in the NA, to the north of 10°N, the data set compiled by Seidov et al. [1996] on the basis of the proxies from Duplessy et al. [1991] and Sarnthein et al. [1995], replaced the CLIMAP SST and modified SSS; (4) present–day and glacial wind stress was extracted from the output of the Hamburg atmospheric circulation model [Lorenz et al., 1996]. The MWE sea surface conditions differ from the LGM ones only in a small area in the NA to the north of approximately 50°N and east of approximately 40°N Further details of the data processing may be found in Seidov et al. [1996].

The horizontal velocity vectors from the OGCM, even if inspected at each level, may be misleading because they do not show vertical motion and do not reflect mixing in the convection chimneys. Hence, the true water motion cannot be appraised from such maps in principle. To visualize true 3–D water motion, we calculate the trajectories of particles that move with the water volumes.

Results

Figure 1 depicts the present day and MWE water volume transport in the upper (Figures 1a and 1c) and in the deep (Figures 1b and 1d) ocean. To get vectors of water transports, the velocity components were multiplied by the side surfaces of the grid cells, and summed vertically from the sea surface to 1.5 km (upper ocean) and from 1.5 km to the bottom (deep ocean). To better illustrate the deep conveyor branch, Figure 2 shows the velocity vectors at 2.5 km depth for the present day (Figure 2a) and MWE (Figure 2b). In our Lagrangian calculations we "deployed" the particles in many areas where the particles can trace the deep conveyor legs. The shaded area in the present–day NNA (at the surface) in Figure 1a and in the MWE deep Indian Ocean (IO) in Figure 1c show the deployment sites chosen for illustration.

Figures 1a, 1b, and 2a picture the present–day conveyor mode with a strong deep ocean flow of NADW which penetrates the ACC, which can be seen to spread farther into the Indian and Pacific oceans. The three–dimensional distribution of the horizontal currents are far more complex than shown in Figure 1. For example, the deep inflow of AABW into the central and North Atlantic is masked in this figure. However, the figure still gives an impression of how different the deep and upper ocean flows are. The deep flows emerge as a truly global coherent feature, justifying, to a certain extent, the term 'conveyor'. The upper ocean circulation system, however, does not appear as a continuous flow system. Instead, the surface basin–scale gyres in different oceans form a chain of gyres that might be hardly viewed as a coherent upper ocean conveyor. Moreover, when considering whether the surface branch of the conveyor is traceable, the time scales of the mixing processes are important. In the deep ocean mixing is weak, and therefore water parcels' properties are preserved for a long time. On the contrary, the characteristics of water traveling in the uppermost (mixing) level are strongly modified by air–sea interactions on a time scale of about two to three months. Therefore, these properties are not necessarily indicative of the conveyor flow.

Some of the particles deployed in the present–day NGS and NNA penetrated into the deep ocean and traveled southward in the western boundary current. Few passed into the South Atlantic, while many remained trapped in the NA subtropical gyre. Many of those which managed to reach the South Atlantic turned back and moved toward NA. About only 10% to 20% of all particles deployed in the shaded area in Figure 1a reached the ACC and were transported farther eastward in this current. Only 2% to 5% of these particles ever emerged in the northern Pacific (one of those particles is shown in Figure 3a). Hence, our study indicates that only a small part of newly formed NADW can physically travel along the whole leg of the deep conveyor. It does not mean that the NADW water cannot reach the Pacific in significant amounts. Note that the operation time of a stable modern–like conveyor can be of several thousand years.

The LGM conveyor (to save space we do not show the LGM maps here) is characterized by a noticeable (more than 40%) decrease in intensity, and deep flows, especially in the NA, take different routes. In comparison to the present day, the NA branch of the glacial conveyor became shallower than at present. However, as in [Seidov et al.,1996], the NA branch of the conveyor still existed at the LGM.

Although the changes in the surface forcing during the MWE are restricted to the NGS and the NNA, the whole deep conveyor from the NA to the eastern Australian coast is affected. NADW production was completely switched off and there was no deep southward flow in the western Atlantic. Moreover, in the MWE experiment there is a reversed deep ocean flow to the north of a substantially curtailed deep ACC in the Indian and Atlantic sectors of the Southern Ocean. Although our calculations do not unambiguously indicate the reversal of the whole deep conveyor branch from the Atlantic to the northern Pacific, the deep flow has indeed an opposite direction over a long distance from the eastern IO to the NNA. Additionally, a deep southward–flowing western boundary current (common to both the LGM and the MWE) is clearly seen in the northern Pacific (Figures 1c and 2b). This flow, which is absent from the present day deep current system, is a possible signature of a reversed Pacific branch of the global conveyor. However, in contrast to the NA boundary currents, simulated changes in the LGM/MWE North Pacific western boundary structure are very poorly constrained, because of the lack of proxy data in this region.

Because deep convection was absent in the NA during the MWE, no trajectory was found to originate in the NNA or NGS and continue into the deep Indian and Pacific Oceans. The reversed deep IO conveyor is best visualized by one of the particles deployed in the deep eastern IO (two are shown in Figure 3b). Another of the shown particles traveled around the globe in the ACC and entered South Atlantic through the Drake Passage, (as in the modern run in Figure 3a; yet no present-day particles showed eastward deep flow in the southern IO). Although some particles crossed the equator, no one of them managed to pass far into the NNA. Hence, despite there was indeed a strong incursion of AABW into the NA, it upwelled mostly to the south of 50°N. Such a southward-shifted density outcrop isolated the NNA from the rest of the World Ocean. Therefore, the driving of the deep ocean circulation during MWE was restricted to the Southern Ocean.

The trajectory–tracing technique may be used to address the ocean ventilation problem. For example, the NA during the MWE is characterized by very old nonventilated intermediate–to–deep water [Sarnthein et al., 1995]. Our Lagrangian calculations show that the MWE deep water in the NA was a mixture of the AABW, originating in the Weddell Sea, and some water sinking in the eastern Indian ocean, which may explain extreme aging of the Atlantic water.

Conclusions

There are several limitations to this rather coarse–resolution modeling. For instance, we were able only to trace the motion within relatively weak (except for ACC) mean flows. Mesoscale eddies, were they resolved, would lead to a dispersion of particles along their paths and might have altered some of the trajectories. However, we have found a reasonable agreement between proxy data and the simulated circulation patterns in a critical region, the North Atlantic, which justifies these coarse–resolution results as a first approximation. We formulate our main conclusions as following:

1. Within the limitations of a coarse–resolution model, we demonstrate that the major meltwater events in the NA might have affected the deep ocean global conveyor substantially and that these changes can be traced in Lagrangian calculations.

2. Based on proxy data which provide realistic glacial and meltwater boundary conditions in the NNA, our combined Eulerian–Lagrangian modeling confirms a weakening and some shallowing of the main conveyor at the LGM and its complete collapse after the very localized post–glacial freshwater discharge in the NNA. The results also show that the water transport during MWE was altered globally.

3. The trajectories imply that the MWE water in the NA was a mixture not only of water originating in the Weddell Sea, but also of some water sinking in the south–eastern IO. It may explain extreme aging of the Atlantic water, stronger than it would be if only the AABW ventilated the NA areas.

Acknowledgments. This study could not have been carried out without the efforts invested by the group at the Geological–Paleontological Institute of Kiel University into paleoreconstructions of the Quaternary North Atlantic. We are especially grateful to Michael Sarnthein for inspiring us to study the meltwater oceanography using the reconstructions provided by the Kiel group. We thank Avan Antia and Karen Bice for their help in improving the language and the style of the manuscript. The comments of two anonymous referees were useful and they are much appreciated. The larger part of the study was accomplished within the framework of the German Climate Program and supported by the Deutsche Forschungsgemeinschaft (DFG) and SFB313 of Kiel University.

References

Broecker, W., The great ocean conveyor, *Oceanography*, *1*, 79–89, 1991.

Broecker, W. S., and G. H. Denton, The role of ocean atmosphere reorganizations in glacial cycles, *Geochim. Cosmochim. Acta*, *53*, 2465–2501, 1989.

Bryan, K., A numerical method for the study of the circulation of the world ocean, J. Comput. Phys., 4, 347–376, 1969.

Climate: Long–Range Investigation Mapping and Prediction (CLIMAP) Project Members, Seasonal reconstructions of the Earth's surface at the Last Glacial Maximum, Map and Chart Ser. MC–36 pp. 1–18, Geol. Soc. of Am., Boulder, Colo., 1981.

Cox, M. D., A primitive equation, 3– dimensional model of the ocean. GFDL Ocean Group Technical Report No. 1, 250 pp., Princeton N.J., 1984.

Drijfhout, S. S., E. Maier–Reimer, and U. Mikolajewicz, Tracing the conveyor belt in the Hamburg large–scale geostrophic ocean general circulation model, J. Geophys. Res., 101, 22,563–22,575, 1996.

Duplessy, J.–C., L. Labeyrie, A. Julliet–Lerclerc, J. Duprat, and M. Sarnthein, Surface salinity reconstruction of the North Atlantic ocean during the last glacial maximum, Oceanol. Acta, 14, 311–324, 1991.

Gordon, A. L., S. E. Zebiak, and K. Bryan, Climate variability and the Atlantic Ocean, *Eos Trans. AGU*, *73*, 161, 164–165, 1992.

Levitus, S., and T. P. Boyer, World Ocean Atlas 1994, vol. 4 (Temperature; 117 pp.). NOAA Atlas NESDIS, Washington., D.C., 1994.

Levitus, S., R. Burgett, and T. P. Boyer, World Ocean Atlas 1994, vol. 3 (Salinity; 99 pp.). NOAA Atlas NESDIS, Washington., D.C., 1994.

Lorenz, S., B. Grieger, P. Helbig, and K. Herterich, Investigating the sensitivity of the atmospheric general circulation Model ECHAM 3 to paleoclimate boundary conditions, Geol. Rundsch., 85, 513–524, 1996.

Pacanowski, R., K. Dixon, and A. Rosati, The GFDL Modular Ocean Users Guide. GFDL Ocean Group Tech. Report No.2, GFDL/NOAA, Princeton University., 1993.

Sarnthein, M. et al., Variations in surface ocean paleoceanography in the Atlantic between 50°N and 80°N: A time–slice record of the last 30,000 years, Paleoceanogr., 10, 1063–1094, 1995.

Seidov, D., M. Sarnthein, K. Stattegger, R. Prien, and M. Weinelt, North Atlantic ocean circulation during the Last Glacial Maximum and subsequent meltwater event: A numerical model, J. Geophys. Res., 101, 16,305–16,332, 1996.

Seidov, D., and B. J. Haupt, Simulated ocean circulation and sediment transport in the North Atlantic during the last glacial maximum and today, Paleoceanography, 12, 281–305 1997.

Toggweiler, J. R., K. Dixon, and K. Bryan, Simulations of radiocarbon in a coarse–resolution world ocean circulation model, 1, Steady state pre–bomb distribution, J. Geophys. Res., 94, 8217–8242, 1989.

B. J. Haupt, Sonderforschungsbereich 313, Universität Kiel, Heinrich–Hecht–Platz 10, D–24118 Kiel, Federal Republic of Germany. (e–mail: bernd@sfb313.uni–kiel.de)

D. Seidov, Earth System Science Center, Pennsylvania State University, University Park, 248 Deike, University Park, PA 16802–2711 USA. (e–mail: dseidov@essc.psu.edu)

(Received April 24, 1997; revised September 22, 1997;
accepted September 30, 1997.)

Paper number 2125

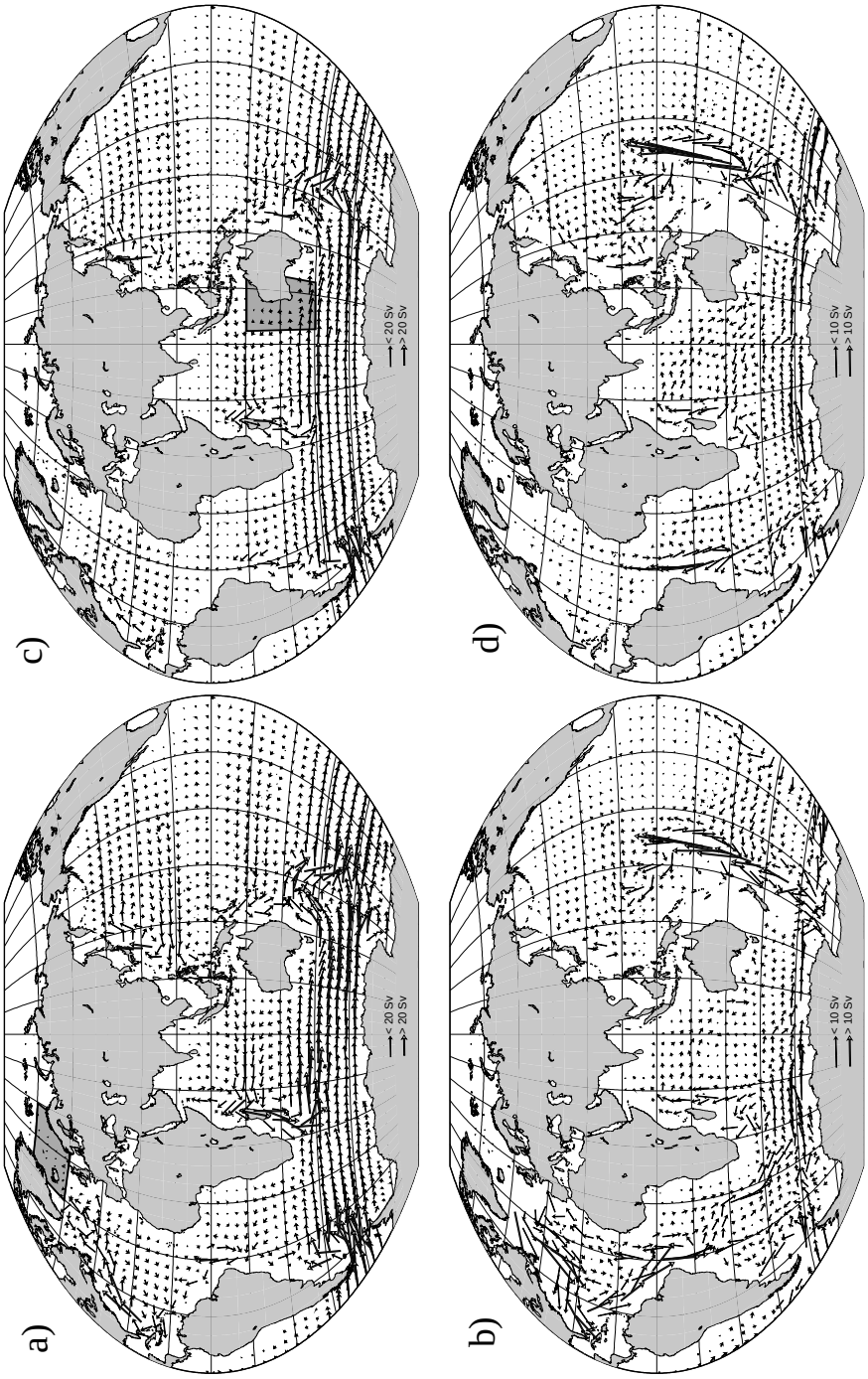

Figure 1. Total water transport across vertical diagonal sections of the grid cells in Sv ($1Sv=10^6$ m^3s^{-1}): a) upper (above 1.5 km) ocean transports at present; b) deep (below 1.5 km) ocean transport at present; b) as in a) for MWE; c) as in b) for MWE. Note different scales of vectors for upper and deep ocean. Shaded areas in Figures 1a and 1c show where the Lagrangian particles are deployed (see text).

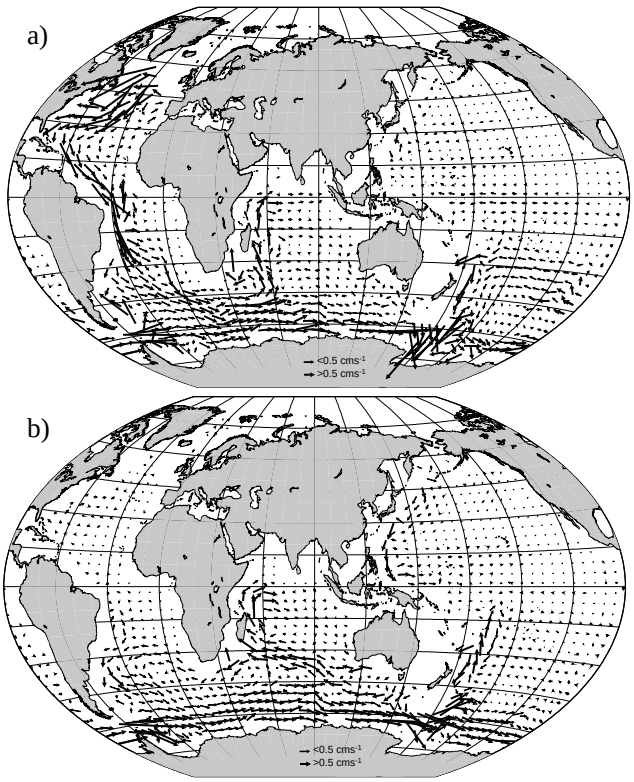

Figure 2. Velocity vectors (in cm s^{-1}) at 2.5 km: a) modern; b) MWE.

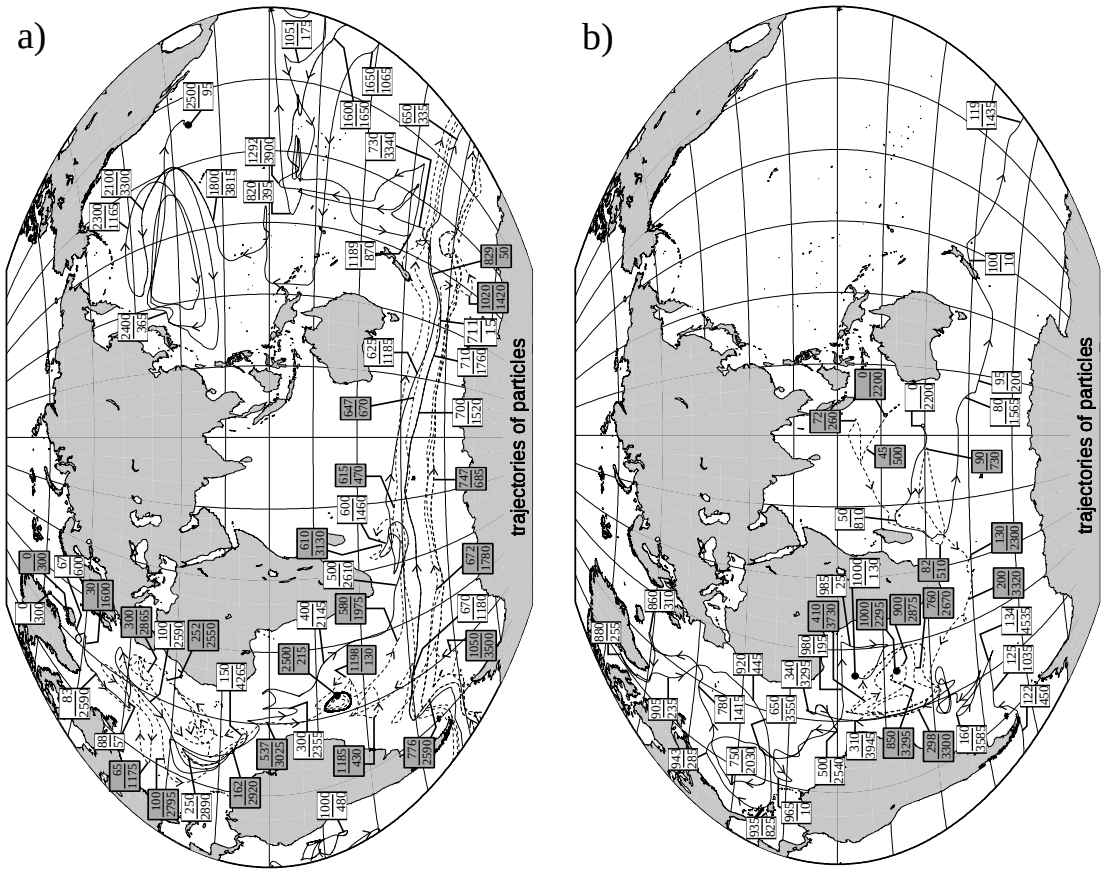

Figure 3. Pairs of trajectories (one trajectory is shown as a solid and the other as a dashed line) visualizing the deep ocean conveyor: a) modern conveyor; b) MWE. The present–day trajectories start at the surface in the NNA, whereas the MWE trajectories start in the deep eastern IO. Small rectangles show time elapsed after deployment (upper numbers) and the depth at which the particle is found on the trajectory at that time.